Advancements in Aerodynamic Shape Optimization with Hybrid Laminar Flow Control for Infinite Swept and Finite Wings at Cruise Conditions

Justin M. Pascual * and David W. Zingg †
Institute for Aerospace Studies, University of Toronto, ON M3H 5T6

Hybrid laminar flow control (HLFC) offers a promising approach to reducing drag by extending laminar flow regions on wings through the combination of passive shaping and active boundary-layer suction. In this work, a suction boundary condition is integrated into a Reynolds-averaged Navier–Stokes aerodynamic shape optimization framework coupled with the SA-sLM2015cc local correlation-based transition model. The implementation is first validated against benchmark cases, including flat-plate flow and NACA 64A010 airfoil experiments, demonstrating accurate prediction of laminar-to-turbulent transition under varying suction intensities. Lift-constrained drag minimization is performed with natural laminar flow, i.e,. without suction, for infinite swept wings under estimated Airbus A340 operating conditions. Applying suction upstream of the transition location on the optimized geometries delays transition, yielding drag reductions of up to 15% relative to fully-turbulent optimized geometries. The updated transition location was determined and suction was also applied just upstream of this location, yielding 19% drag reduction compared to a turbulent optimized geometry.

Nomenclature

A	airfoil area
b	span
c	chord
C_D	coefficient of drag
C_L	coefficient of lift
C_Q	coefficient of suction
e	total energy per unit volume
j	mass flux
l	length of suction zone for a flat plate
$\dot{m}$	mass flow rate per unit area
M	Mach number
Q_{suc}	total volumetric flow rate through the surface
$\mathbf{Q}_{\text{target}}$	solution vector of the conservative flow variables at an individual node
Re	Reynolds number
v_{suc}	suction speed
v_{w}	normal component of velocity
U_∞	free-stream velocity
Λ	sweep angle
μ_∞	free-stream dynamic viscosity
ρ	density
ρ_w	local density at the wall
ρ_∞	free-stream density
ξ	curvilinear coordinate

*PhD Candidate, University of Toronto Institute for Aerospace Studies, AIAA Student Member, justin.pascual@mail.utoronto.ca
†Distinguished Professor of Computational Aerodynamics and Sustainable Aviation, University of Toronto Institute for Aerospace Studies, AIAA Associate Fellow, david.zingg@utoronto.ca

I. Introduction

The commercial aviation industry has experienced significant growth over recent decades. This growing demand has heightened environmental concerns, driving interest in the development of more efficient aircraft designs. Aerodynamic shape optimization supports this effort by iteratively simulating and refining designs to improve specific performance metrics, offering a more systematic and effective alternative to traditional manual design iteration methods.

For a typical commercial aircraft, viscous drag contributes roughly 50% of the overall drag while operating at cruise conditions [1]. As flow passes over a surface, it transitions from laminar to turbulent, with turbulent flow having higher frictional forces and a thicker boundary layer, increasing the overall drag. There are two main mechanisms through which flow transitions on commercial aircraft, the first being Tollmien-Schlichting (TS) instabilities, which occur in two-dimensional boundary layers in the form of vortices aligned in the spanwise direction. TS instabilities are highly receptive to disturbances in the flow and can be amplified as they are advected downstream, resulting in transition to turbulence [2]. The second mechanism is crossflow (CF) instabilities, which can arise on swept wings and are characterized by an inflection point in the transverse velocity profile. This inflection point causes the flow to be unstable, resulting in streamwise vortices that transition the flow to turbulence.

To delay transition from laminar to turbulent flow, flow control methods can be implemented to push the transition location further downstream thereby increasing the regions of laminar flow [3]. One promising passive approach is natural laminar flow (NLF), which relies on wing shaping to extend the laminar region. However, NLF design is generally restricted to modest sweep angles and Reynolds numbers [4, 5]. At higher sweep angles and Reynolds numbers, active laminar flow control becomes necessary. HLFC extends NLF by adding boundary-layer suction to the passive aerodynamic shaping used in NLF. This combination enables significantly greater control over the boundary-layer profile, allowing transition to be pushed farther downstream. The technique is particularly suited to wings and empennages due to their large wetted areas and typically high sweep, while nacelles and other components may rely on other drag-reduction strategies [6].

The concept of applying suction across the full upper and lower surfaces of a wing was experimentally explored by NACA in the Langley low-turbulence pressure tunnel [7]. Using a NACA 64A010 airfoil with a sintered bronze perforated surface, the study demonstrated that boundary-layer suction could maintain laminar flow at low speeds ($M \approx 0.3$) and moderate Reynolds numbers ($Re = 6 \times 10^6$). NASA later extended these investigations in the Langley Laminar-Flow-Control Experiment [8–11], applying suction over both upper and lower wing surfaces of a supercritical airfoil in unswept and swept configurations. The study validated transition prediction methods and compared slotted and perforated suction surfaces, accounting for temperature gradients and surface porosity in the efficiency calculations. Results showed that suction could successfully delay transition up to 60% of the chord, confirming the effectiveness of both suction surface types in moving the transition location downstream. Building on these experimental studies, Fisher and Fischer demonstrated active laminar flow control on a JetStar aircraft during the Leading-Edge Flight Test (LEFT) [12]. The aircraft employed both slotted and perforated suction surfaces, with additional measures such as Krueger flaps with integrated deicer nozzles to protect against insect, ice, and particulate contamination. Both suction configurations were successfully implemented, with slotted surfaces proving more effective at delaying transition, while perforated surfaces were more prone to clogging.

Numerical studies of HLFC have also been undertaken. Sudhi et al. applied active laminar flow control to two-dimensional airfoils using XFOIL coupled with the e^N transition prediction method [13]. Drag-minimization optimizations were performed with and without suction, treating the onset of suction as a design variable. Optimized suction distributions applied upstream of the natural transition location delayed transition to 80% of the chord and reduced drag by 30% relative to the no-suction case. Extending this methodology, Sudhi et al. explored HLFC on transonic, infinite swept wings at high Reynolds numbers [13]. By jointly optimizing wing shape and suction distribution using a multi-objective genetic algorithm, HLFC configurations achieved up to 25% drag reduction over NLF designs at $Re = 30 \times 10^6$ and sweep angle 22.5°, outperforming fully turbulent designs by 27%. Prasannakumar et al. [14] applied suction to a finite wing swept at 16° at the operating conditions of a hybrid-electric propulsion aircraft. The aircraft had a cruise Mach number of 0.71, $C_L = 0.5$ and a range of 4600 km. The objective of this work was to maximize the laminar region while minimizing the suction and pressure drag through the control of suction panels at different spanwise stations at the leading edge. The results of this study indicate that the transition point is able to be moved to 60% chord with considerations for a battery powering the suction system to maximize the net drag reduction.

Pascual and Zingg [15] implemented a suction-based aerodynamic optimization framework for HLFC, coupling a suction boundary condition with the SA-sLM2015cc transition model [16, 17] in a Reynolds-averaged Navier–Stokes (RANS) solver. Strategically placing multiple suction locations yielded significant drag reductions. On an NLF-optimized RAE2822 airfoil with operating conditions: $M = 0.6$, $Re = 10 \times 10^6$, $C_L = 0.42$, suction applied upstream

of the transition location reduced drag by 6% at a suction speed of 0.1% U_∞. For infinite swept wings with operating conditions: $M = 0.78$, $Re = 15 \times 10^6$, $C_L = 0.492$, $\Lambda = 25°$, aerodynamic shaping alone achieved 5% drag reduction, while applying suction upstream at a suction speed of 0.1% U_∞, resulted in 8% drag reduction, validating the ability of the methodology to simulate the flow physics of suction and the effect of suction on laminar-turbulent transition.

The objective of the current work is to develop an effective methodology to perform aerodynamic shape optimization in the presence of laminar-turbulent transition and suction, and to use the optimization methodology developed to study optimal approaches to drag reduction via HLFC and to quantify the performance benefits achievable. To validate the suction boundary condition implementation, several benchmark cases are examined, including flat-plate flow, airfoil experiments, and high-speed swept-wing configurations.

Section II outlines the flow solver, transition-prediction model, and aerodynamic shape optimization framework, including the modeling of active laminar flow control. Section III presents the validation cases performed on flat plates and airfoils. Section IV presents the results of lift-constrained drag minimization of two-dimensional airfoils with and without sweep and finite wings, incorporating suction in various ways. Finally, conclusions and future work are presented in Section V.

II. Methodology

Aerodynamic shape optimization is carried out using Jetstream, the high-fidelity optimization framework developed at the University of Toronto Institute for Aerospace Studies. Jetstream comprises five core components: a Newton-Krylov-Schur flow solver for the Reynolds-Averaged Navier–Stokes (RANS) equations [18, 19]; a transition-prediction model based on empirical local correlations, coupled with the one-equation Spalart–Allmaras (SA) turbulence model [16]; a unified geometry parameterization and mesh deformation scheme based on linear elasticity [20]; the SNOPT gradient-based optimizer used alongside a discrete-adjoint gradient method [21]; and a combination of free-form deformation (FFD) and axial deformation for geometry control [22]. The framework has been extended to support active boundary-layer suction through the implementation of a suction boundary condition.

The flow solver, Diablo [19], is a multiblock, parallel, implicit RANS solver that employs second-order summation-by-parts (SBP) operators for spatial discretization and uses simultaneous approximation terms (SATs) to enforce boundary and block-interface conditions.

Geometry parametrization and mesh deformation follow the approach of Hicken and Zingg [20], in which each computational block is associated with a B-spline volume whose surface control points provide a low-dimensional representation of the geometry. Mesh motion is propagated to the interior using a linear-elasticity formulation. Geometry modification uses a hybrid strategy combining free-form and axial deformation methods [22]. Free-form deformation (FFD) volumes govern section shape, chord, and twist through B-spline control points, while axial B-spline curves control sweep, span, and dihedral. For the infinite swept-wing cases considered here, axial-curve deformation is unnecessary but is included for completeness and applied in the finite-wing optimizations.

Gradient-based optimization is performed using SNOPT [21], which implements a sequential quadratic programming (SQP) framework capable of handling linear and nonlinear constraints. Gradients are supplied via the discrete-adjoint method [23, 24].

A. Transition Prediction Model

The flow solver incorporates boundary-layer transition prediction using the SA-sLM2015cc model developed by Piotrowski and Zingg [16, 17]. This model builds on the γ-$Re_{\theta t}$ framework; an empirical, correlation-based approach introduced by Langtry and Menter [25] to model TS and CF instabilities that includes two transport equations: one for γ, the intermittency function, and another for $Re_{\theta t}$, the momentum-thickness Reynolds number. The SA-sLM2015 model [16] couples this transition framework with the one-equation Spalart–Allmaras turbulence model [26], and replaces non-smooth functions in the original formulation with smooth alternatives to ensure a continuous and differentiable design space. Piotrowski and Zingg later enhanced the model by incorporating compressibility corrections for both TS and CF instabilities, leading to the current version, SA-sLM2015cc [17].

B. Suction Boundary Condition

In this work, active boundary-layer suction is incorporated into the optimization framework through the definition of a suction velocity at the surface. The design process accounts for viscous effects, including the additional drag and pump power associated with suction, by introducing appropriate penalty terms in the objective function. The porosity

Table 1 Inflow conditions for flat plate with boundary-layer suction

Case	C_Q	v_w (m/s)
1	8.33×10^{-4}	- 0.03342
2	4.16×10^{-3}	- 0.16712

of the surface is also considered, allowing for a physically consistent representation of the suction mechanism and its impact on the flow.

1. Suction Drag Considerations

The suction boundary condition formulation accounts for the drag effects introduced by active boundary-layer control. The suction drag represents the additional skin-friction component arising from the extraction of low-momentum fluid near the surface, which alters the boundary-layer velocity profile and increases the local wall shear stress. Following Fehrs [27], the suction drag coefficient over a unit surface is expressed as:

$$C_{D,\text{suc}} = \frac{2 \cdot D_{\text{suc}}}{\rho_\infty U_\infty^2 bl} = -2 \cdot \frac{v_w}{U_\infty} = 2 \cdot C_Q. \tag{1}$$

This formulation relates the prescribed suction velocity to the additional skin-friction drag.

2. Suction Pump Power Considerations

Active suction requires energy to sustain the prescribed mass flux through the porous surface, which can be expressed as an equivalent power drag coefficient. Following the formulation of Prasannakumar et al. [28] and assuming the pump efficiency, $\eta_p = 1$, the ideal suction pump power penalty is given by:

$$C_{D,\text{pump}} = \left(\frac{U_e}{U_\infty}\right)^2 \left(\frac{v_{\text{suc}}}{U_\infty}\right). \tag{2}$$

This expression captures the energy cost of suction in a compact form, allowing it to be directly incorporated into aerodynamic optimization as an equivalent drag contribution.

III. Model Validation

This section presents the validation of the developed suction boundary condition. Two validation cases are discussed: boundary-layer suction applied to a flat plate and to a NACA 64A010 airfoil, demonstrating agreement with both computational and experimental reference data.

A. Boundary-layer Suction Applied to a Flat Plate

Fehrs implemented a no-slip wall boundary condition using an effusion mass flux boundary condition in the DLR TAU-Code [27] and validated it analytically. The operating conditions consist of $U_\infty = 40$ m/s, $Re = 6.62 \times 10^6$ with the suction coefficient and suction velocity listed in Table 1. The results in Fig 1 show the velocity profiles with respect to the similarity variable η, which is defined as:

$$\eta = y\sqrt{\frac{U_\infty}{2\nu x}}.$$

The present computational results show excellent agreement with the reference data.

B. Flow over an Airfoil with Prescribed Suction

Braslow et al. conducted experiments using a NACA 64A010 airfoil with a sintered bronze surface through which suction was applied [7]. Suction was applied across the entirety of the upper and lower surfaces, aside from a small portion at the leading edge at approximately 5% x/c. The wind tunnel was operated at a speed of $M \approx 0.3$ and

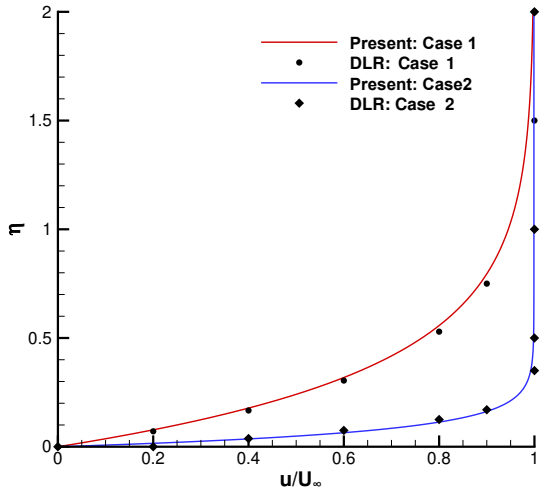

Fig. 1 Boundary-layer velocity profiles with two different suction coefficients produced using the SA-sLM2015cc transition model validated against DLR TAU-Code computational results (shown with symbols).

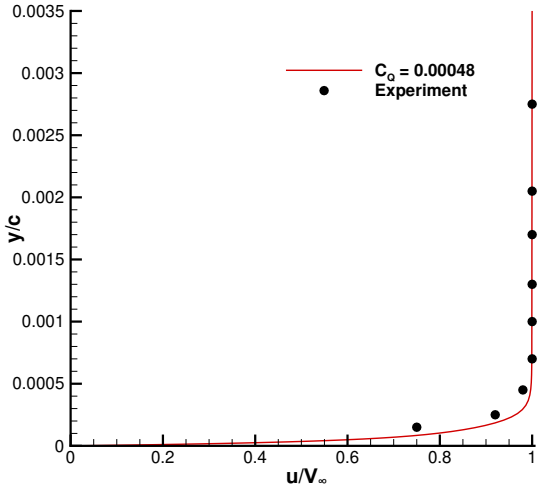

Fig. 2 Boundary-layer velocity profiles at 83% chord comparing results obtained with the SA-sLM2015cc transition model to the NACA 64A010 wind tunnel experiment.

$Re = 6 \times 10^6$ and the airfoil was fixed at $\alpha = 0°$. The computational mesh used for this validation case is a 270×182 O-grid.

The experiment measured the boundary-layer profiles at 83% of the chord and found that the flow was able to remain laminar. The results of this validation case are shown in Figure 2, with the computational results showing a laminar boundary-layer profile in agreement with the experimental results.

With the same experimental operating conditions, geometry and suction application, Schwartzberg et al. captured boundary-layer profiles for several suction coefficients and analyzed the effect this variation had on the transition front [29]. Fehrs also used the DLR-TAU code to replicate this experiment [27]. To compare against experimental data, the transition location for $C_Q = 0$ is first matched, and to account for the surface roughness, Fehrs used a turbulence intensity of $Tu = 0.6\%$. The cases run in the present work use a turbulence intensity of $Tu = 0.63\%$. The results comparing the

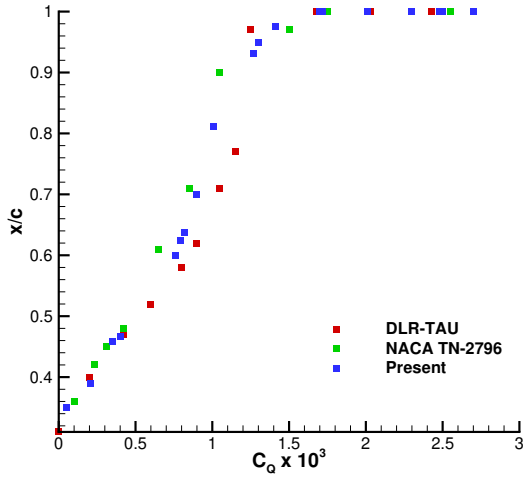

Fig. 3 Extent of laminar flow on the upper surface of a NACA 64A010 airfoil. Suction is applied across the entirety of the upper surface, except for the first 5% chord with various suction coefficients used.

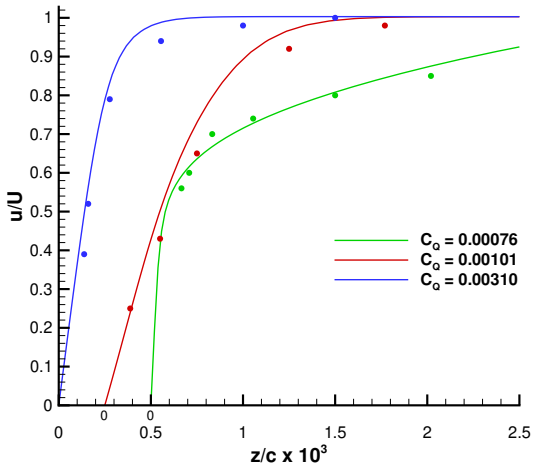

Fig. 4 Boundary-layer profiles for a NACA 64A010 airfoil. The profiles are taken on the upper surface at 75% chord comparing experimental results (shown with symbols) with the present work for various suction coefficients.

computational and experimental transition locations are plotted in Figure 3 with the present work demonstrating close agreement with both the experimental and the computational results. Boundary-layer profiles were captured as part of this experiment and are shown in Figure 4, comparing the experimental results with the present work. When a lower suction velocity of $C_Q = 0.00076$ is used, the profile has a thicker profile, which is more characteristic of a turbulent boundary-layer profile. When suction is increased to a velocity of $C_Q = 0.00101$, a transitional boundary-layer profile is obtained. At a suction velocity of $C_Q = 0.00310$, a thinner profile is obtained which is characteristic of a laminar boundary-layer profile. These results show close agreement with the experimental values, providing validation for the current methodology.

IV. Optimization Results

The methodology is applied to aerodynamic optimization studies involving infinite swept wings, where suction is applied to optimized geometries through discrete slot implementations. This study aims to quantify the aerodynamic performance improvements achievable through the integration of active laminar flow control into the design process.

A. Suction Applied to an Optimized Geometry at Airbus A340 Operating Conditions

The following cases were completed using the RAE2822 airfoil as the initial geometry at estimated Airbus A340 conditions consisting of $M = 0.82$, $Re = 45.34 \times 10^6$, $C_L = 0.512$, $\Lambda = 30°$. The computational meshes used for the infinite swept wing cases are 360×120 O-grids. This geometry has 11 free-form deformation control points for each surface. Suction is applied at a fixed location on a geometry obtained from a lift-constrained drag minimization without suction, subject to an area constraint and minimum thickness constraints. The NLF optimization problem is summarized as:

$$\begin{aligned} \min_{\mathbf{X}} \quad & C_D(\mathbf{X}) \\ \text{s.t.} \quad & C_L = 0.512 \\ & A \geq A_{\text{init}} \\ & t/c \geq 0.15(t/c)_{\text{init}}, \end{aligned} \tag{3}$$

where $\mathbf{X}$ represents the design variable vector, including the angle of attack and the FFD control points, C_L and C_D the lift and drag coefficients, respectively, A the cross-sectional area, and t/c the thickness-to-chord ratio for each FFD control point pair. The 'init' subscript indicates the value of the quantity from the baseline geometry. Previous results by Pascual and Zingg [15] investigated lower sweep angle and Reynolds number combinations. The present work shifts focus to conditions where aerodynamic shaping offers limited benefits, increasing reliance on active suction to delay transition and reduce drag. The presented cases account for the suction drag penalty defined in Equation 1, with suction being applied over the entire leading edge up until the upper and lower surfaces' respective transition locations on the optimized geometry.

Results for the initial geometry analysed with transition prediction, a fully-turbulent optimized geometry for comparison, the NLF optimized geometry, and three different suction coefficients applied to the NLF optimied geometry are shown in Table 2. Figure 5 shows the pressure coefficient plot for the baseline, NLF-optimized, and suction configurations. As seen in the table, the NLF optimization provides an 5.7% reduction in drag relative to the turbulent optimized geometry, but the optimizer struggles to significantly delay transition, especially on the lower surface. When suction is introduced, the aerodynamic performance improves further. Even the lowest suction level tested ($C_Q = 0.0001$) provides a drag reduction of 10.9% compared to the turbulent optimized case. Increasing the suction coefficient consistently enhances the delay of transition, with $C_Q = 0.0010$ producing a 14.9% drag reduction. Figure 6 illustrates the influence of suction on the transition location for both surfaces. As expected, higher suction velocities push the transition point further downstream. However, the incremental benefit decreases with increasing C_Q, indicating diminishing returns in transition delay at higher suction levels.

1. Application of Suction at the Updated Transition Location

Following the analysis in the previous section with suction applied to the leading edge, suction was then applied beginning approximately 3% upstream of each newly identified transition point. The resulting suction extents and corresponding drag levels are summarized in Table 3 and the pressure distributions shown in Figure 7. Figure 8 illustrates that transition on the upper surface is displaced downstream for all suction levels, with larger shifts occurring at higher C_Q. This delay in transition produces a corresponding reduction in drag, with a suction coefficient value of $C_Q = 0.0010$, producing a drag reduction of 14.9% relative to the fully turbulent optimized airfoil.

V. Conclusions

In this paper, we present a framework for aerodynamic shape optimization incorporating HLFC through suction. The methodology was first validated against benchmark cases including flat-plate flow and NACA 64A010 airfoil experiments, demonstrating accurate prediction of laminar-to-turbulent transition and suction effects. The validated methodology was used to investigate the drag reduction potential of HLFC at Airbus A340 operating conditions. First NLF optimization is performed but given the high Reynolds number and sweep angle, limited amounts of laminar

Table 2 Summary of results for the Airbus A340 case with suction applied along the entire leading edge, extending to 9% of the chord on the upper surface and 2.5% on the lower surface. Percent drag reduction is shown compared to the turbulent optimized case.

Configuration	C_D (counts)	L/D	Transition Location (x/c)	
			Upper Surface	Lower Surface
Baseline	70.8	72.4	4.4%	2.2%
Turbulent Optimized	66.5	77.1	-	-
NLF Optimized	62.4 (-5.7%)	82.0	9.2%	2.6%
Suction Coefficient				
C_Q = 0.0001	59.2 (-10.9%)	87.7	15.0%	3.8%
C_Q = 0.0005	57.3 (-13.8%)	92.2	19.6%	6.4%
C_Q = 0.0010	56.6 (-14.9%)	94.4	21.0%	8.3%

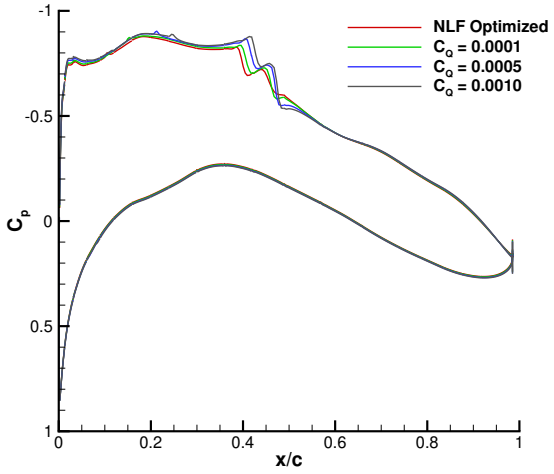

Fig. 5 Pressure coefficient plot at Airbus A340 operating conditions with suction applied along the entire leading edge, extending to 9% of the chord on the upper surface and 2.5% on the lower surface.

Table 3 Summary of results for the Airbus A340 case in which suction was applied along the entire leading edge extending to 9% chord on the upper surface and 2.5% on the lower, and then also applied starting 3% upstream of the updated transition location for each suction coefficient. Percent drag reduction is shown compared to the turbulent optimized case.

Suction Coefficient	Additional Suction Location (x/c)		C_D (counts)	Transition Location (x/c)	
	Upper Surface	Lower Surface		Upper Surface	Lower Surface
C_Q = 0.0001	12.0% – 15.0%	2.5% – 3.7%	58.46 (-12.1%)	15.6%	4.0%
C_Q = 0.0005	16.5% – 19.5%	3.5% – 6.5%	55.71 (-16.2%)	21.3%	7.9%
C_Q = 0.0010	18.0% – 21.0%	5.3% – 8.3%	53.79 (-19.1%)	21.0%	15.3%

flow can be achieved. Suction is applied ~~to~~ the resulting airfoils, moving transition aft, yielding 15% drag reductiono compared with a turbulent optimized geometry. A second application of suction applied just upstream of these transition

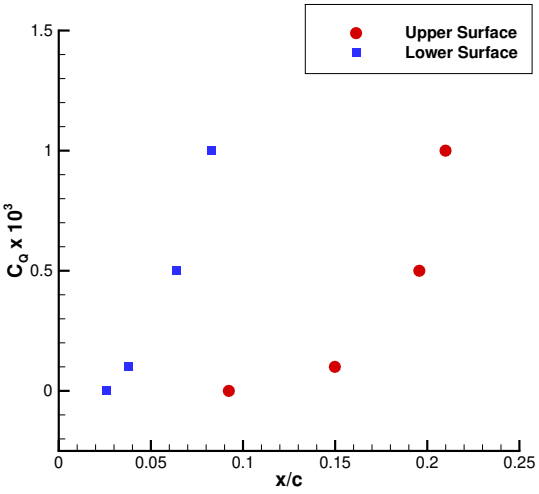

Fig. 6 Transition location on the upper and lower surface at Airbus A340 operating conditions for various suction velocities when applied to the optimized geometry.

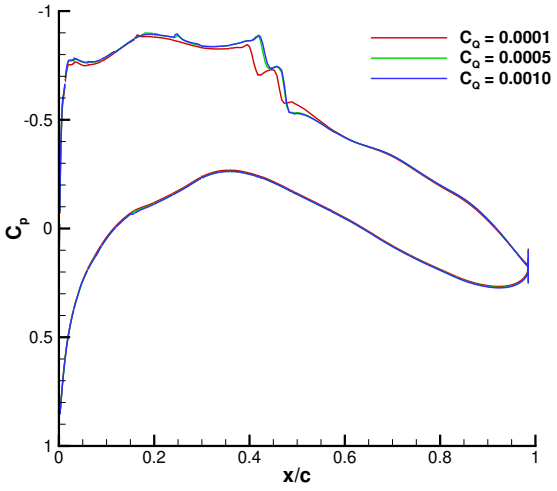

Fig. 7 Pressure coefficient plot at Airbus A340 operating conditions with suction applied along the entire leading edge, extending to 9% of the chord on the upper surface and 2.5% on the lower surface.

locations pushes transition even further aft, yielding 19% drag reduction compared to a turbulent optimized geometry.

Future work will focus on extending this framework to finite wings to capture realistic planform effects and full spanwise flow behavior. Optimization of suction power and placement will also be incorporated to identify the most effective combination of suction intensity and location for drag reduction while minimizing energy expenditure. These developments will enable more realistic assessments of HLFC performance for practical aircraft configurations and support the design of efficient suction-based laminar flow control systems.

Acknowledgements

This work is partially funded by Bombardier, Transport Canada, the Natural Sciences and Engineering Research Council (NSERC), and the University of Toronto. All results in this paper were computed on the Niagara and Trillium

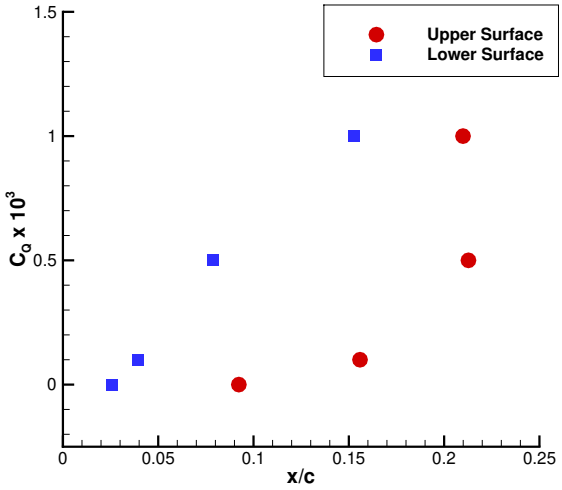

Fig. 8 Transition location on the upper and lower surface at Airbus A340 operating conditions for various suction velocities when applied to the NLF optimized geometry with suction also applied just upstream of the updated transition location ~~with an extent of 3%~~.

supercomputers at the SciNet HPC Consortium, a part of the Digital Research Alliance of Canada.

References

[1] Bushnell, D., "Overview of Aircraft Drag Reduction Technology," *AGARD Report 786*, 1992.

[2] Green, J. E., "Civil Aviation and the Environment – The Next Frontier for the Aerodynamicist," *The Aeronautical Journal*, Vol. 110, No. 1110, 2006, pp. 469–486. https://doi.org/10.1017/S0001924000001378.

[3] Green, J. E., "Civil Aviation and the Environmental Challenge," *The Aeronautical Journal*, Vol. 107, No. 1072, 2003, pp. 281–299. https://doi.org/10.1017/S0001924000013579.

[4] Lynde, M. N., and Campbell, R. L., "Computational Design and Analysis of a Transonic Natural Laminar Flow Wing for a Wind Tunnel Model," *35th AIAA Applied Aerodynamics Conference, AIAA Paper 2017-3058*, American Institute of Aeronautics and Astronautics, Denver, Colorado, 2017. https://doi.org/10.2514/6.2017-3058.

[5] Lynde, M. N., Campbell, R. L., Rivers, M. B., Viken, S. A., Chan, D. T., Watkins, A. N., and Goodliff, S. L., "Preliminary Results from an Experimental Assessment of a Natural Laminar Flow Design Method," *AIAA Scitech 2019 Forum, AIAA Paper 2019-2298*, American Institute of Aeronautics and Astronautics, San Diego, California, 2019. https://doi.org/10.2514/6.2019-2298.

[6] Johansen, J., and Sørensen, J. N., "Prediction of Laminar/Turbulent Transition in Airfoil Flows," *Journal of Aircraft*, Vol. 36, No. 4, 1999, pp. 731–734. https://doi.org/10.2514/2.2501.

[7] Braslow, A., Burrows, D., Tetervin, N., and Visconti, F., "Experimental and Theoretical Studies of Area Suction for the Control of the Laminar Boundary Layer on an NACA 64A010 Airfoil," Tech. Rep. Report 1025, NACA, 1951.

[8] Bobbitt, P. J., Ferris, J. C., Harvey, W. D., and Gordia, S. H., "Results for the Hybrid Laminar Flow Control Experiment," , No. NASA-TM-107582, 1992.

[9] Harvey, W. D., Harris, C. D., Brooks, C. W., Clukey, P. G., and Stack, J. P., "Design and Experimental Evaluation of a Swept, Supercritical LFC Airfoil," *Langley Symposium on Aerodynamics*, Vol. 1, 1986.

[10] Dagenhart, J. R., "Design of a Laminar-Flow-Control Supercritical Airfoil for a Swept Wing," *NASA, Langley Research Center, Hampton, VA, USA, CTOL Transport Technology*, 1978.

[11] Berry, S., Dagenhart, J. R., Brooks, C. W., and Harris, C. D., "Boundary-layer Stability Analysis of Langley Research Center 8-foot LFC Experimental Data," *NASA, Langley Research Center, Hampton, VA, USA, Research in Natural Laminar Flow and Laminar-Flow Control, Part 2*, 1987.

[12] Fisher, D. F., and Fischer, M. C., "Development Flight Tests of JetStar LFC Leading-edge Flight Test Experiment," *NASA, Langley Research Center, Research in Natural Laminar Flow and Laminar-Flow Control, Part 1*, 1987.

[13] Sudhi, A., Radespiel, R., and Badrya, C., "Design Exploration of Transonic Airfoils for Natural and Hybrid Laminar Flow Control Applications," *J. Aircr.*, Vol. 60, No. 3, 2023, pp. 716–732.

[14] Prasannakumar, A., Sudhi, A., Seitz, A., and Badrya, C., "Design of Hybrid-Laminar-Flow-Control Wing and Suction System for Transonic Midrange Aircraft," *Journal of Aircraft*, Vol. 61, No. 3, 2024, pp. 709–732. https://doi.org/10.2514/1.C037398.

[15] Pascual, J. M., and Zingg, D. W., "Progress in the Application of an Aerodynamic Shape Optimization Capability using Hybrid Laminar Flow Control to Airfoils and Infinite Swept Wings," *AIAA SCITECH 2025 Forum, AIAA Paper 2025-0484*, American Institute of Aeronautics and Astronautics, Reston, Virginia, 2025.

[16] Piotrowski, M. G. H., and Zingg, D. W., "Smooth Local Correlation-Based Transition Model for the Spalart–Allmaras Turbulence Model," *AIAA Journal*, Vol. 59, No. 2, 2021, pp. 474–492. https://doi.org/10.2514/1.J059784.

[17] Piotrowski, M., and Zingg, D., "Compressibility Corrections to Extend a Smooth Local Correlation-based Transition Model to Transonic Flows," *The Aeronautical Journal*, Vol. 127, No. 1313, 2023, pp. 1141–1170. https://doi.org/10.1017/aer.2022.105.

[18] Hicken, J. E., and Zingg, D. W., "Parallel Newton-Krylov Solver for the Euler equations Discretized Using Simultaneous Approximation Terms," *AIAA Journal*, Vol. 46, No. 11, 2008, pp. 2773–2786. https://doi.org/10.2514/1.34810.

[19] Osusky, M., and Zingg, D. W., "A Parallel Newton-Krylov-Schur Flow Solver for the Navier-Stokes Equations Discretized using Summation-by-Parts Operators," *AIAA Journal*, Vol. 51, No. 12, 2008, pp. 2833–2851.

[20] Hicken, J. E., and Zingg, D. W., "Aerodynamic Optimization Algorithm with Integrated Geometry Parameterization and Mesh Movement," *AIAA Journal*, Vol. 48, No. 2, 2010, pp. 400–413. https://doi.org/10.2514/1.44033.

[21] Gill, P. E., Murray, W., and Saunders, M. A., "SNOPT: An SQP Algorithm for Large-Scale Constrained Optimization," *SIAM Journal on Optimization*, Vol. 12, No. 4, 2002, pp. 979–1006. https://doi.org/10.1137/S1052623499350013.

[22] Gagnon, H., and Zingg, D. W., "Two-Level Free-Form and Axial Deformation for Exploratory Aerodynamic Shape Optimization," *AIAA Journal*, Vol. 53, No. 7, 2015, pp. 2015–2026. https://doi.org/10.2514/1.J053575.

[23] Jameson, A., Martinelli, L., and Pierce, N. A., "Optimum Aerodynamic Design using the Navier-Stokes Equations," *Theor. Comput. Fluid Dyn.*, Vol. 10, No. 1-4, 1998, pp. 213–237.

[24] Osusky, L., Buckley, H., Reist, T., and Zingg, D. W., "Drag minimization based on the Navier–Stokes equations using a Newton–Krylov approach," *AIAA J.*, Vol. 53, No. 6, 2015, pp. 1555–1577.

[25] Langtry, R. B., and Menter, F. R., "Correlation-Based Transition Modeling for Unstructured Parallelized Computational Fluid Dynamics Codes," *AIAA Journal*, Vol. 47, No. 12, 2009, pp. 2894–2906. https://doi.org/10.2514/1.42362.

[26] Spalart, P. R., and Allmaras, S. R., "A One-equation Turbulence Model for Aerodynamic Flows," *La Recherche Aerospatiale*, , No. 1, 1994, pp. 5–21.

[27] Fehrs, M., "Boundary Layer Suction Modeling based on the DLR TAU-code Effusion Mass Flux Boundary Condition," *Notes on Numerical Fluid Mechanics and Multidisciplinary Design*, Notes on numerical fluid mechanics and multidisciplinary design, Springer International Publishing, Cham, 2020, pp. 175–184.

[28] Prasannakumar, A., Wolff, J., Radespiel, R., Boermans, L., Hühne, C., and Badrya, C., "Design and Power Calculation of HLFC Suction System for a Subsonic Short-range Aircraft," *CEAS Aeronautical Journal*, Vol. 13, No. 4, 2022, pp. 1003–1026. https://doi.org/10.1007/s13272-022-00614-1.

[29] Schwartzberg, M., and Braslow, A., "Experimental Study of the Effects of Finite Surface Disturbances and Angle of Attack on the Laminar Boundary Layer of an NACA 64A010 Airfoil with Area Suction," Tech. Rep. TN-2796, NACA, 1952.